Anisotropy in Turbulent Drag Reduction

P. Tong,[1,4] W. I. Goldburg,[2] J. S. Huang,[1] and T. A. Witten[1,3]
[1]*Exxon Research and Engineering Company, Annandale, New Jersey 08801*
[2]*Department of Physics and Astronomy, University of Pittsburgh, Pittsburgh, Pennsylvania 15260*
[3]*The James Franck Institute, University of Chicago, 5640 S. Ellis Avenue, Chicago, Illinois 60637*
[4]*Department of Physics, Oklahoma State University, Stillwater, Oklahoma 74078*
(Received 24 May 1990; revised manuscript received 5 October 1990)

We have studied turbulent drag reduction using the technique of photon-correlation homodyne spectroscopy to measure turbulent velocity gradients in a dilute polymer solution. A large anisotropic suppression of turbulent velocity differences is found in the bulk region of the turbulent fluid and along the direction of the mean flow. The suppression effect is associated with an enhancement of the turbulent drag reduction. This anisotropy caused by polymer molecules in turbulent flow may be important in understanding turbulent drag reduction.

PACS numbers: 47.50.+d, 42.20.−y, 47.25.−c, 61.25.−f

There are many fascinating flow phenomena in polymeric fluids. Turbulent drag reduction in dilute polymer solutions is one of them.[1] Trace amount of flexible polymers in solution can significantly reduce the drag of turbulent flow below that for the solvent alone. The drag reduction has important applications which have stimulated many experimental and theoretical studies in past decades.[1-3] However, the mechanism for the drag reduction is not well understood, and only tentative explanations exist. It is believed that turbulent flow strongly stretches polymer chains in the solution, and the reaction of the stretched polymer chains to the flow gives rise to the drag reduction.[2,4-7]

In this Letter we report an experimental study of turbulent drag reduction using the novel technique of photon-correlation homodyne spectroscopy[8] to measure velocity gradients in a turbulent polymeric fluid. In contrast to most previous experimental studies, which have focused on the straight pipe system due to its obvious applications, we have studied turbulent flow in a concentric cylindrical cell in which the inner cylinder rotates. The outer cylinder was made of Plexiglas to admit the incident light and observe the scattering. The outer cylinder was 12.7 cm both in height and in inner diameter. The inner rotating cylinder was a smooth brass tube, 9.4 cm in height and 5.7 cm in diameter. To generate more turbulence we deliberately inserted four radial baffle plates placed symmetrically on the wall of the outer cylinder (see Fig. 1). The width of each baffle plate was 1.3 cm, and its height was 12.7 cm. Later on we will discuss the turbulent velocity field in the cell with and without baffles.

The polymer used in this study was polyethylene oxide (PEO), a commonly used water-soluble drag-reducing agent. The polymer powder was premixed in distilled water at the desired concentration. Fresh samples were used to avoid possible chemical degradation. Nominal molecular weight of the PEO sample was 5×10^6, and the molecular-weight distribution was broad. Using the dynamic light-scattering technique[8] we measured the hydrodynamic radius R_h of the polymer chain to be R_h =74 nm. The measured viscosity η of the PEO solution at the concentration c=55 ppm (parts per million by weight) was $1.08\eta_w$, where η_w=0.01 P is the viscosity of water.

We first describe the measurements of the autocorrelation function of the scattered light intensity $I(t)$. The cylindrical cell was filled with a fluid (water or the PEO solution) seeded with small polystyrene latex spheres (with diameters of 0.1 μm), which follow the local flow and scatter light. The volume fraction of the seed particles was $\sim10^{-4}$. At this volume fraction the particle mean spacing is much larger than their diameter (dilute solution) but is much smaller than the smallest turbulent scale. The focused laser beam from a 1-W argon-ion laser (λ_0=515 nm) entered the cell, and a lens imaged the thin laser beam without magnification onto a slit. The slit limited the length of the thin laser beam viewed by a photomultiplier. The photomultiplier was located far behind the slit, and its output pulses went to a digital correlator whose output gives the homodyne autocorrela-

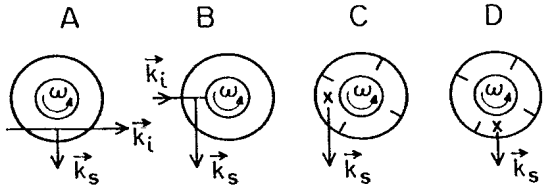

$(\frac{\partial v_r}{\partial \phi}+\frac{\partial v_\phi}{\partial \phi})\frac{L}{d}$; $(\frac{\partial v_r}{\partial r}+\frac{\partial v_\phi}{\partial r})L$; $(\frac{\partial v_z}{\partial z}+\frac{\partial v_\phi}{\partial z})L$; $(\frac{\partial v_z}{\partial z}+\frac{\partial v_r}{\partial z})L$

FIG. 1. The top view of the flow cells and the scattering geometries (z axis is perpendicular to the paper). $\mathbf{k}_i$ denotes the incident wave vector, $\mathbf{k}_s$ the scattering wave vector, and × the incident position of the vertical laser beam. The components of velocity gradients probed in each geometry are also listed, where d is the distance between the laser beam and the rotation axis.

tion function,[8] $g(t)=\langle I(0)I(t)\rangle=\langle I^2\rangle[1+BG(qt,L)]$. Here B is a constant which depends on the geometry of the experimental setup. Measurements were made at room temperature and at the scattering angle $\theta=90°$.

It has been shown[9,10] that the correlation function $G(qt,L)$ senses the velocity difference $\mathbf{V}(R,t)$ of pairs of points in the turbulent fluid separated by a distance R. In the turbulent fluid the motion of the seeded particles Doppler shifts the scattered light. Therefore the phase of the detected light is modulated (due to frequency beating) at a frequency equal to the difference in Doppler shifts of all particle pairs in the scattering volume. The function $G(qt,L)$ has the form

$$G(qt,L)=\int_0^L dR\,h(R)\int_{-\infty}^{\infty} dV\,P(V,R)\cos(qtV)\,, \quad (1)$$

where $h(R)=2(1-R/L)/L$ is the fraction of particle pairs separated by a distance R in the thin scattering volume of length L. In the above, $P(V,R)$ is the probability distribution function of $V(R,t)$, where $V(R,t)$ is the component of $\mathbf{V}(R,t)$ along the scattering vector $\mathbf{q}$. The amplitude of $\mathbf{q}$ is $q=(4\pi/\lambda)\sin(\theta/2)$, where λ is the wavelength of the light in the fluid.

The function $G(qt,L)$ yields information about the velocity difference in the direction of $\mathbf{q}$ and at scale L. A characteristic decay time τ of $G(qt,L)$ can be defined as $\tau=\int_0^\infty dt\,G(qt,L)$. This definition of τ emphasizes the initial decay of $G(qt,L)$ governed by the slit width L. With a simple dimensional argument we can show that τ is proportional to $[qu(L)]^{-1}$, where $u(L)$ is the characteristic velocity difference at scale L. More than a thousand correlation functions have been measured in both the baffled cell and the unbaffled cell in order to map out the turbulent velocity field and to observe the effect of the polymer on velocity gradients. The function $G(qt,L)$ was measured as a function of the rotation speed ω ($\omega=2\pi f$; f in turns per second), the slit width L, and the spatial position of the laser beam in the flow cell. The direction of the incident beam was varied in three directions: the azimuthal (ϕ) direction (A in Fig. 1), the radial (r) direction (B in Fig. 1), and the vertical (z) direction. In the latter case we employed two scattering geometries by changing the incident position of the vertical beam in the cell (C and D in Fig. 1). In Fig. 1 we also list the components of the velocity gradients probed in each geometry. Notice that $G(qt,L)$ measures velocity gradients through the term $\mathbf{q}\cdot\mathbf{u}(L)$.

The measurements of $G(qt,L)$ in the unbaffled cell reveal that in our working range of ω (up to 262 Hz), the predominant turbulent velocity gradient is in the horizontal (r,ϕ) plane, and the strongest velocity gradient in this plane is in the radial direction. When the laser beam enters the cell vertically, the measured $G(qt,L)$ is insensitive to the change of L, but is a strong function of the beam diameter. This suggests that the velocity difference over the beam diameter ($\sim$0.1 mm) is larger than that over a vertical distance L ($\sim$1.0 mm). The decay time τ of the $G(qt,L)$ measured in geometry A is approximately 2 times larger than that measured in geometry B. In the baffled cell, on the other hand, one can clearly see velocity fluctuations in the z direction. When the fluid hits the corner where the outer wall and the baffle plate meet, its flow direction is forced to change either in the horizontal plane (where the fluid element has to be stretched) or in the vertical direction (up-down motion). This vertical motion was seen by visual observation of the fluid motion as well as by the correlation measurements (strong L dependence of the decay time τ). A typical value of τ for water in the baffled cell is of the order of 1 μsec. This corresponds to a velocity difference of 4.4 cm/sec at the scale of 1 mm.

The measured $G(qt,L)$ also shows that in the baffled cell the velocity gradient in the r direction is reduced while in the ϕ direction it is approximately the same as in the unbaffled cell. Thus the insertion of the baffle plates enhances the velocity fluctuation in the z direction and reduces the velocity gradient in the r direction. We should emphasize that the turbulence in the baffled cell is neither homogeneous nor isotropic at the scale of $\sim$1 mm. One may view the turbulence in the baffled cell as a turbulent wake generated by the baffle plates. Furthermore, this turbulent wake is steady and spatially extends to the bulk region of the gap between the two cylinders. More detailed discussions on the turbulent field will be reported elsewhere.[11]

The measurement of $G(qt,L)$ in the unbaffled cell shows that the addition of the PEO polymer in water suppresses turbulent velocity gradients in the horizontal (r,ϕ) plane. Figure 2 compares the measured $G(qt,L)$ in water (open symbols) and in the 55-ppm PEO solution (solid symbols). The upper two curves were obtained

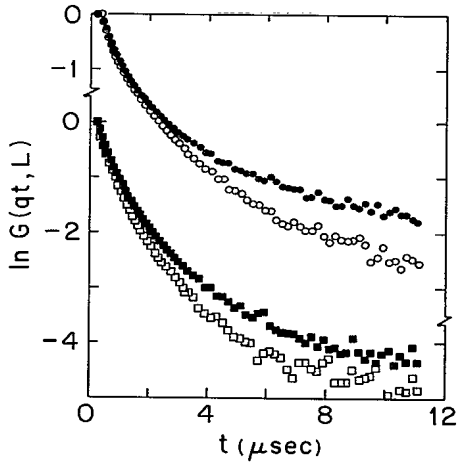

FIG. 2. The measured $G(qt,L)$ in the unbaffled cell for water (open symbols) and for the 55-ppm PEO solution (solid symbols). The upper two curves were measured when $\omega=209$ Hz and $L=0.6$ mm in the scattering geometry B. The lower two curves were measured when $\omega=262$ Hz and $L=1.0$ mm in the scattering geometry A.

when $\omega = 209$ Hz and $L = 0.6$ mm in the scattering geometry B. Though the viscosity of the two fluids is almost the same, $G(qt,L)$ in the PEO solution decays slower than in water; the decay time τ in the PEO solution being increased by $\sim 20\%$. This suppression effect is seen for several slit widths from 0.2 to 1.4 mm. When the laser beam enters the cell along the ϕ direction (geometry A), a similar suppression effect was observed, but the effect is smaller. The suppression effect was enhanced when ω was increased from 209 to 262 Hz in the unbaffled cell. The lower two curves in Fig. 2 show the measured $G(qt,L)$ in the scattering geometry A when $\omega = 262$ Hz, $L = 1.0$ mm. No suppression effect was observed when the incident beam is along the z direction (geometry C, no baffles) for various ω up to 262 Hz. The measured $G(qt,L)$ in water and in the PEO solution are the same. This is because vertical velocity fluctuations are absent in the unbaffled cell.

In the baffled cell, however, we did observe the suppression of velocity gradients by addition of a polymer in the scattering geometry C. This suggests that the polymer molecules suppress the vertical velocity fluctuations produced by the baffle plate. The upper two curves in Fig. 3 show the measured $G(qt,L)$ in water (open circles) and in the PEO solution (solid circles) when $\omega = 203$ Hz and $L = 0.5$ mm. The position of the vertical beam was 1.5 cm away from the edge of a baffle plate in the downstream direction and 1.3 cm away from the outer wall (see geometry C in Fig. 1). The decay time τ in the PEO solution is increased by $\sim 40\%$. This suppression effect is seen for several slit widths from 0.2 to 1.5 mm. The maximum suppression effect in this scattering geometry occurs in the near baffle region (~ 1.3 cm away from the *outer* wall in the downstream direction) where the vertical velocity fluctuations are the strongest. When the scattering geometry is changed to D, the measured $G(qt,L)$ in water and in the PEO solution remain the same for various L and ω. This is shown by the lower two curves in Fig. 3 ($\omega = 203$ Hz, $L = 0.5$ mm). We notice that the decay time τ of $G(qt,L)$ measured in water and in geometry C is 50% shorter than in geometry D when $\omega = 203$ Hz and $L = 1.0$ mm.

A slightly larger suppression effect is also observed in the baffled cell when the laser beam enters the cell along the ϕ direction at $\omega = 209$ Hz. As mentioned above, the turbulent velocity in the ϕ direction is approximately the same for both the baffled and the unbaffled cells, and hence one expects a qualitatively similar suppression effect in both cells. The slightly larger effect in the baffled cell indicates that in the cell the turbulent velocity gradient is enhanced in the mean flow direction. The difference in $G(qt,L)$ between water and the PEO solution disappeared when the scattering geometry was changed to B. This can be understood by the fact that the turbulent velocity gradients in the radial direction are reduced in the baffled cell. The data in Figs. 2 and 3 thus reveal a large anisotropic suppression of turbulent velocity differences in the polymer solution. In particular, as shown in Fig. 3, polymer molecules suppress the velocity difference $(\partial v_\phi/\partial z)L$, but not the other two components listed under the geometries C and D in Fig. 1.

We turn next to the measurements of the wall stress T_w (force per unit area) on the rotating cylinder in both the unbaffled cell and the baffled cell. The purpose of the measurement was to relate the observed suppression of velocity gradients in the PEO solution with the turbulent drag reduction. A torque-sensitive permanent-magnet dc motor was used to drive the inner rotating cylinder. The driving current was directly measured using a 6.5-digit voltmeter. For the permanent-magnet dc motor, the driving current is proportional to the torque exerted on the rotating cylinder. The actual rotating frequency was measured by strobe light. Figure 4(a) shows the measured T_w in the unbaffled cell as a function of ω for three solutions: distilled water (solid circles), 25

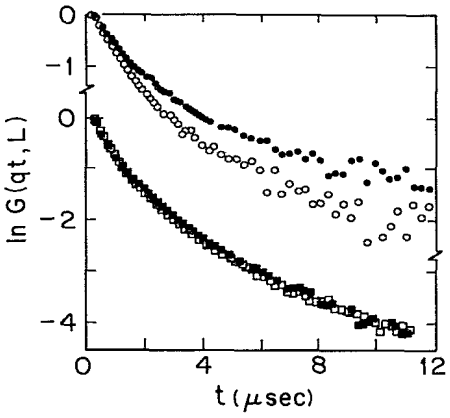

FIG. 3. The measured $G(qt,L)$ in the baffled cell for water (open symbols) and for the 55-ppm PEO solution (solid symbols) when $\omega = 203$ Hz and $L = 0.5$ mm. The upper two curves were measured in the scattering geometry C. The lower two curves were measured in the scattering geometry D.

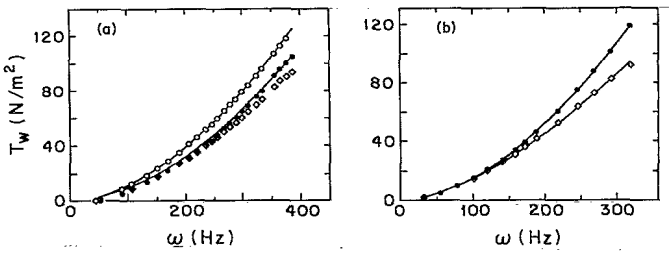

FIG. 4. The measured T_w as a function of ω for three solutions: distilled water (solid circles), 25 wt% glycerol aqueous solution (open circles), and the 55-ppm PEO solution (diamonds). (a) The measured T_w in the unbaffled cell. The solid curves are the fits by Eq. (2) with $\alpha = 0.2$. (b) The measured T_w in the baffled cell. The upper solid curve is a fit by Eq. (2) with $\alpha = 0.2$, and the lower solid curve is the fit with $\alpha = 0.4$.

wt% glycerol aqueous solution (open circles), and the PEO aqueous solution with $c=55$ ppm (diamonds). An onset of the drag reduction appears to occur at $\omega_0 \simeq 250$ Hz. The 25 wt% glycerol solution ($\eta=2.08\eta_w$) was used to check the viscosity dependence of the wall stress.

In our measurements ω ranged from 42 to 385 Hz. The corresponding Reynolds number $\mathrm{Re}_a=\omega a^2/\nu$ is in the range 3.3×10^4 to 3×10^5, where a ($=2.8$ cm) is the radius of the inner rotating cylinder, and ν is the kinematic viscosity of water. To judge the effect of the turbulent shear $S(\mathbf{r})$ on the polymer chains, one has to compare $S(\mathbf{r})$ with the polymer relaxation rate $\Gamma=(k_BT/6\pi\eta_w)R_h^{-3}$. In the strong-shear region, where $S(\mathbf{r})>\Gamma$, the shear will strongly stretch the polymer chain, and this stretching is believed to be responsible for the onset of the drag reduction. From the Kolmogorov theory,[12] the maximum turbulent shear rate $S(l_d)\simeq\nu\mathrm{Re}^{3/2}/l_0^2$, where l_d ($\simeq l_0\mathrm{Re}^{-3/4}$) is the viscous dissipation length, and l_0 is a characteristic size of the system (we take $l_0=a$). In analyzing the turbulence near the wall one should use a Reynolds number Re_δ which is based on the turbulent boundary-layer thickness δ rather than Re_a. The two Reynolds numbers can be related by the empirical equation[13] $\mathrm{Re}_\delta=0.37\mathrm{Re}_a^{4/5}$. One can estimate the onset frequency ω_0 by equating $S(l_d)$ to Γ. For our polymer with $R_h=74$ nm, we obtain $\omega_0\simeq220$ Hz which agrees with the measurement.

From turbulent boundary-layer theory[13] the wall stress is

$$T_w\sim\rho U^2(\mathrm{Re}_a)^{-\alpha}\sim\rho^{1-\alpha}\eta^\alpha U^{2-\alpha}a^{-\alpha}\equiv A\omega^{2-\alpha}, \qquad (2)$$

where $U=a\omega$ is the characteristic velocity, and ρ is the density of the fluid. A typical value of α is 0.2. Equation (2) is an empirical scaling law, which holds for the turbulent wall stress on many smooth surfaces. Our measured T_w for distilled water and the 25 wt% glycerol solution ($\eta=2.08\eta_w$) are found to be well fitted by Eq. (2) with $\alpha=0.2$ [solid curves in Fig. 4(a)]. The coefficient A was obtained from the power-law fitting, and the ratio of the two coefficients $\beta=A_{\mathrm{PEO}}/A_{\mathrm{water}}=1.19$. From Eq. (2) one expects the ratio $\beta=(\rho/\rho_w)^{0.8}(\eta/\eta_w)^{0.2}=1.20$, which agrees well with our drag measurement.

Figure 4(b) shows the measured T_w in the baffled cell as a function of ω for distilled water (solid circles) and the PEO aqueous solution with $c=55$ ppm (diamonds). One can clearly see an enhancement of the drag reduction at large ω. For the largest accessible ω ($=310$ Hz), we obtain a 25% drag reduction, which is approximately 3 times larger than in the unbaffled cell. Another important change is that in this cell the onset rotating frequency ω_0 is greatly reduced. It is notable that T_w in the baffled cell is 55% larger than that in the unbaffled cell, so the flow field is clearly changed by the baffles. Yet, the exponent α in Eq. (2) has the same value in both cells filled with water or the glycerol solution. However, for the PEO solution the exponent α changes its value to $\alpha=0.4$ in the baffled cell [the lower solid curve in Fig. 4(b)].

In conclusion, a large anisotropic suppression of turbulent velocity gradients is found in the dilute PEO solution. This suppression effect is associated with an enhancement of the turbulent drag reduction. The maximum suppression occurs in the bulk region of the turbulent fluid and along the mean flow direction. Furthermore, the suppression of velocity differences is found at the scale of ~1 mm, which is much larger than the Kolmogorov dissipation length l_d (<0.04 mm). The experiment reveals that the dominant polymer effect is on the velocity component along the mean flow direction. Gradients of this component appear to be suppressed in all directions in which the gradients are substantial. This effect presumably arises from the elastic stress in the polymer chains opposing the stretching and shearing of fluid elements.

We would like to thank A. Libchaber, E. Herbolzheimer, and D. Peiffer for useful discussions, and K. R. Sreenivasan for illuminating correspondence. This work was supported in part by the National Science Foundation under Grant No. DMR-8914351.

[1]P. S. Virk, AIChE J. **21**, 625 (1975).

[2]J. L. Lumley, Annu. Rev. Fluid Mech. **1**, 367 (1969); J. Polym. Sci. Macromol. Rev. **7**, 263 (1973).

[3]W.-M. Kulicke, M. Kotter, and H. Grager, Adv. Polym. Sci. **89**, 1 (1989).

[4]G. Ryskin, Phys. Rev. Lett. **59**, 2059 (1987); J. Fluid Mech. **178**, 423 (1987).

[5]M. Tabor and P. G. de Gennes, Europhys. Lett. **2**, 519 (1986); P. G. de Gennes, Physica (Amsterdam) **140A**, 9 (1986).

[6]M. T. Landahl, Phys. Fluids **20**, S55 (1977).

[7]J. L. Lumley and I. Kubo, in *The Influence of Polymer Additives on Velocity and Temperature Fields,* edited by B. Gampert (Springer-Verlag, Berlin, 1984), p. 3.

[8]B. J. Berne and R. Pecora, *Dynamic Light Scattering* (Wiley, New York, 1976).

[9]P. Tong, W. I. Goldburg, C. K. Chan, and A. Sirivat, Phys. Rev. A **37**, 2125 (1988); P. Tong and W. I. Goldburg, Phys. Fluids **31**, 2841 (1988).

[10]P. J. Bourke *et al.*, J. Phys. A **3**, 216 (1970).

[11]P. Tong, W. I. Goldburg, J. S. Huang, and T. A. Witten (to be published)

[12]A. N. Kolmogorov, C. R. Dokl. Acad. Sci. URSS **30**, 301 (1941); **31**, 538 (1941).

[13]H. Schlichting, *Boundary-Layer Theory* (McGraw-Hill, New York, 1979), 7th ed.